Asociación Argentina
de Mecánica Computacional

Mecánica Computacional Vol XXIX, págs. 8391-8409 (artículo completo)
Eduardo Dvorkin, Marcela Goldschmit, Mario Storti (Eds.)
Buenos Aires, Argentina, 15-18 Noviembre 2010

NUMERICAL STUDY OF THE EFFECTS OF BONDING LAYER PROPERTIES ON ELECTRICAL SIGNATURES OF PIEZOELECTRIC SENSORS

Hector A. Tinoco[a], Alberto L. Serpa[b], Angel M. Ramos[c]

[a]*Department of Mechanical Engineering, Autonomous University of Manizales-UAM, Old Train Station, Manizales (Caldas), Colombia. andrest149@gmail.com, http://www.autonoma.edu.co*

[b]*Department of Computational Mechanics, Faculty of Mechanical Engineering, University of Campinas-UNICAMP, 13083-970 Campinas-SP, Brazil. serpa@fem.unicamp.br, http://www.fem.unicamp.br*

[c]*Departament of Applied Mathematics, Complutense University of Madrid, Madrid 28040, Spain. angel_Ramos@mat.ucm.es, http://www.ucm.es*

Keywords: Piezoelectric sensor, adhesive layer, finite element method, debonding

Abstract. A numerical study is carried out to understand adhesive layer effects on the electromechanical coupling of piezoelectric sensors bonded to structures. This study shows that electrical signatures depend on the bonding conditions along the interface structure/adhesive/sensor. A mathematical model for electrical signatures was established using the Maxwell's equation (Gauss law for electricity). The mechanical analysis was defined considering only shear deformation along the adhesive layer. Numerical solutions were obtained by the finite element method and compared with analytical solutions. The analytical solution was provided by solving differential equations in terms of displacements. Results indicate that the thickness and length of the adhesive layer have significant effects on electrical signatures and these effects can be applied to detect debonding of piezoelectric sensors.

Copyright © 2010 Asociación Argentina de Mecánica Computacional http://www.amcaonline.org.ar

1 INTRODUCTION

Piezoelectric transducers have begun to increase in popularity in different areas of structural mechanics in the last few years. They are used as sensors and as actuators in smart structures. Piezoelectric transducers are available in many ways and shapes (PI ceramics, 2010). Most extensively, piezoelectric transducers are used in the form of thin sheets which can be bonded or embedded in structures by means of an adhesive layer. They are used to measure directly the local dynamic and static response of a structure. When the structure is stressed mechanically, the piezoelectric material bonded to the structure acts to produce an electrical charge (piezoelectric sensor). On the other hand, a mechanical strain through the piezoelectric material is produced when an electrical field is applied along the perpendicular plane which presents a dipole (piezoelectric actuator).

Especially, in the last few years, piezoelectric transducers have been widely used in structural health monitoring (SHM) for damage detection in structures (Park et al. 2000; Ritdumrongkul et al. 2004; Xu et al. 2004; Yang et al. 2006), nondestructive evaluation (NDE) (Tanasoiu et al. 2002), nondestructive inspection (NDI) (Diamanti et al. 2007) and applications of several types in structural engineering (Sun et al. 1995; Giurgiutiu and Zagrai, 2000; Bhalla and Soh, 2004a,b).

Electrical signatures of piezoelectric sensors are emitted depending on deformation conditions as it is related in constitutive equations (see Eq. (1)). Mechanical and electrical relations in piezoelectric elements bonded to structures are determined by electro-mechanical coupling. An analytical and experimental development was presented by (Crawley and De luis, 1987). They used piezoelectric materials as elements of smart structures. A scaling analysis was performed to demonstrate that the effectiveness of a piezoelectric actuator is independent of the structure size. An analysis of the electro-mechanical coupling of piezoelectric actuators integrated in mechanical systems was realized by (Liang et al. 1993). This study determined the actuator power consumption and energy transfer in electro-mechanical systems. The study of electro-mechanical coupling in piezoelectric transducers and structures leaded to introduce a new concept of coupling relating the mechanical impedance of the structure with the electro-mechanical impedance of the piezoelectric transducer. This concept is called electro-mechanical impedance and was introduced by (Liang et al. 1996). These studies did not consider the adhesive layer between the interface structure/piezoelectric transducer.

The electric behavior of piezoelectric transducers bonded to structures as strain sensors was investigated by (Sirohi and Chopra, 2000). Strain was measured in terms of electrical charge generated by piezoelectric transducer as a result of the direct piezoelectric effect. In this reference, strain through the piezoelectric sensor was considered constant and the piezoelectric transducer was modeled as a capacitor and the adhesive layer was not considered.

Other models have been established to study electro-mechanical coupling between piezoelectric transducers and structures considering the adhesive interface. A modified model of the electro-mechanical impedance of piezoelectric sensor and actuator was presented by (Xu and Liu, 2002). The model considered the adhesive interface between a piezoelectric patch and a

Copyright © 2010 Asociación Argentina de Mecánica Computacional http://www.amcaonline.org.ar

structure. Complete mechanical system (structure / adhesive / piezoelectric) was established as a spring-mass-damper system for carrying out the electro-mechanical analysis. The effect of bonding layer on dynamic interaction between piezoelectric actuator-sensors and structures was thus taken into account in this reference. (Balla and Soh, 2004) analyzed the force transfer mechanism through the adhesive layer at the adhered interface. Force transmission between the structure and the piezoelectric element occurs through the bonding layer, via shear stress mechanism. Force transference at the adhesive interface by means of shear stresses causes a shear lag effect in the ends of the piezoelectric sensor.

In this research it is shown that the adhesive interface can significantly modify the measured electro-mechanical. The dynamic behavior of piezoelectric sensors depends on the bonding condition along the interface between sensors and structures. The effects of the adhesive layer on the dynamic behavior were studied by (Han et al. 2008). Results indicate that the mechanical properties of the adhesive layer present significant effects on electrical responses of the sensor.

Numerical models have also been developed using the finite element method (FEM) as an approximation to coupled electro-mechanical solutions. An important model for vibration analysis using tetrahedral piezoelectric elements was established by (Henno and Huges 1970). They introduced the concept of 'static condensation of the electric potential degrees of freedom', which presents the electric potential and loads written in terms of the mechanical properties of the structure. An approach of a piezoelectric finite element was also carried out by (Tzou and Tseng, 1990). In this study some applications of dynamic measurements and control of structures were shown. Some finite element formulations for piezoelectric elements were derived from the principle of virtual work and were verified mathematically and numerically by (Chen et al. 1996). A thin solid plane element with 4 degrees of freedom per node, 12-nodes triangular was formulated by (Tzou and Ye, 1996). They used shape functions quadratic in the two in-plane directions and linear in the transverse direction with the assumption of a layerwise constant shear angle (Mindlin hypothesis). Other formulations to beams including the adhesive effect were proposed by (Tylinkowski, 1993; Pietrzakowski, 2000; Benjeddou and Trindale, 2001). Most recently a finite element model of smart beams with distributed piezoelectric elements was proposed by (Bendary et al., 2010).

This study presents a static and dynamic analytical model which represents the deformations of a piezoelectric sensor bonded to a structure, considering its adhesive interface. FEM was used to determine the deformations in different cases of adhesion (sensor partially bonded). Results obtained from analytical model were compared with numerical solutions obtained by FEM with (COMSOL, 2007). The effects of the geometric properties of adhesive layer on the mechanical and electrical behavior of the sensor are the principal aims of this work. For instance, in this study it is shown that partially debonding is not necessarily considered as a failure. Therefore, it is very important to understand theoretically which are the effects of the mechanical properties of the adhesive layer on electrical signatures emitted by the piezoelectric sensor. Comprehension of bonding layer effects can be used for detecting debonding and to evaluate sensor performance.

Copyright © 2010 Asociación Argentina de Mecánica Computacional http://www.amcaonline.org.ar

2 ELECTROMECHANICAL ANALISYS

2.1 Piezoelectric sensor

The mathematical model, which represents electro-mechanical coupling in piezoelectric materials (PI ceramics, 2010), is expressed by the constitutive equations

$$T_{ij} = c_{ijkl}S_{kl} - e_{ijk}E_k,$$
$$D_i = e_{ikl}S_{kl} + \varepsilon_{ik}E_k, \tag{1}$$

where, S_{kl} is the strain vector (6×1) (dimensionless), D_i (C/m²) is the electric displacement of size (3×1), E_k (V/m) is the applied electric field vector (3×1), T_{ij} (N/m²) is the mechanical stress vector (6×1), ε_{ik} (F/m) is the dielectric constant of the piezoelectric material (3×3), e_{ikl} (3×6) and e_{ijk} (6×3) are piezoelectric constants (C/m^2) and c_{ijkl} (N/m²) is the elastic matrix (6×6).

Using constitutive equations (see Eq. (1)), the equation of the piezoelectric sensor (see (Yang and Ngoi, 1999)) is established of the following form (electric field is not applied in the piezoelectric material, $E_k = 0$)

$$T_{ij} = c_{ijkl}S_{kl},$$
$$D_i = e_{ikl}S_{kl}. \tag{2}$$

2.2 Coupled static model

Figure 1 presents a piezoelectric transducer used as a sensor bonded to a structure. The piezoelectric sensor is bonded to a structure by means of an adhesive layer. The adhesive layer provides the mechanical force transference between the structure and the PZT sensor.

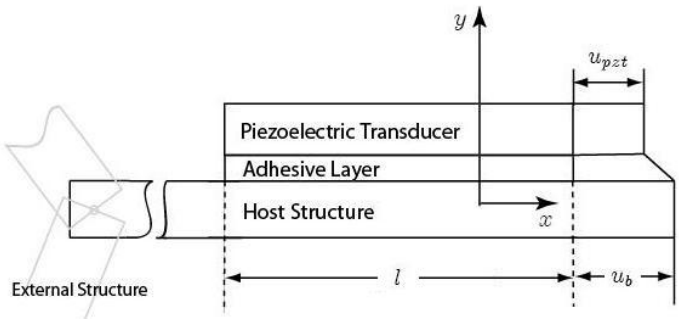

Figure 1: Axial deformation of structure-adhesive layer-PZT

When the structure is axially loaded, the phenomenon of axial deformation in the structure / bonding layer / piezoelectric (PZT) sensor is shown in Fig. 1. Force transference from the structure to the PZT sensor is carried out via shear forces. u_{pzt} and u_b represent displacements

Copyright © 2010 Asociación Argentina de Mecánica Computacional http://www.amcaonline.org.ar

of the PZT sensor and of the structure after applying the force P to the structure. The reference system is established in the following form: the x-direction is located in $l/2$ and at the y-direction is located in $h_s/2$, l is the length of the PZT sensor and h_s is the thickness of the structure.

In order to establish the static equilibrium of the set shown in Fig. 1, it should be defined a differential element at a x distance of each section of the structure, adhesive layer and PZT sensor. Force diagrams are shown in Fig. 2.

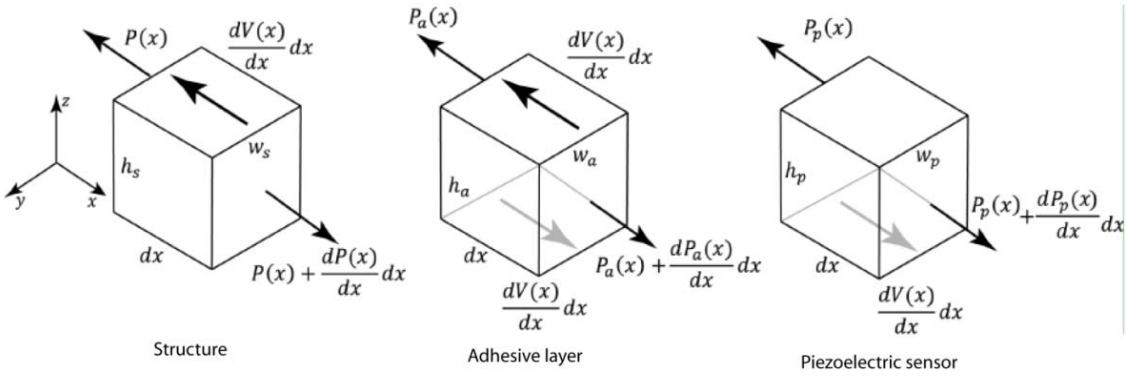

Figure 2: Differential elements structure-adhesive layer-PZT

It is necessary take into account the following considerations for determining the equilibrium: $\frac{dV(x)}{dx}dx = \tau(x)w_a dx$, where $V(x)$ and $\tau(x)$ are the shear force and the shear stress through interfaces structure ⁄ bond layer ⁄ PZT sensor. Then, $\tau(x)$ can be approximated by

$$\tau(x) = G_a \frac{u_b(x) - u_{pzt}(x)}{h_a}, \tag{3}$$

where h_a is the thickness of the adhesive layer, G_a is the shear modulus of the adhesive layer.

The coupled differential equations obtained from differential elements (see Fig. 2) are given by

$$\frac{d^2u_b(x)}{dx^2} - \frac{G_a}{h_a E_s h_s}u_b(x) = -\frac{G_a}{h_a E_s h_s}u_{pzt}(x),$$

$$\frac{d^2u_{pzt}(x)}{dx^2} - \frac{G_a}{h_a E_p h_p}u_{pzt}(x) = -\frac{G_a}{h_a E_p h_p}u_b(x), \tag{4}$$

Copyright © 2010 Asociación Argentina de Mecánica Computacional http://www.amcaonline.org.ar

The following boundary conditions are applied to Eq. (4),

$$u_b(-l/2) = u_0, \frac{du_{pzt}(-l/2)}{dx} = 0, \quad \frac{du_b(l/2)}{dx} = \frac{P}{E_s w_s h_s}, \qquad \frac{du_{pzt}(-l/2)}{dx} = 0,$$

where E_s is the elasticity modulus of the structure, h_p is the thickness of the PZT sensor and E_p is the elasticity modulus of the PZT sensor. It is important to mention that for obtaining equations (4) some considerations as $w_a = w_s = w_p$ were carried out, where w_a, w_s, w_p are the width of the adhesive layer, the structure and the PZT sensor.

The solutions for coupled differential equations (see Eq. (4)) are determined by

$$\begin{aligned} u_{pzt}(x) &= c_1 + c_2 x + c_3 \cosh(\beta x) + c_4 \sinh(\beta x), \\ u_b(x) &= c_1 + c_2 x + A(c_3 \cosh(\beta x) + c_4 \sinh(\beta x)). \end{aligned} \tag{5}$$

To obtain deformations from Eq. (5), the definition of strain $\left(\epsilon = \frac{du}{dx}\right)$ can be applied. The constants are determined by

$$\beta = \sqrt{k_1 + k_2}, \tag{6}$$

where $k_1 = \frac{G_a}{h_a E_s h_s}$, $k_2 = \frac{G_a}{h_a E_p h_p}$, $A = 1 - \frac{\beta^2}{k_2}$. Constants c_1, c_2, c_3 and c_4 are determined by the application of boundary conditions.

2.2 Coupled dynamic model

The dynamic model is established using the same elements of Fig. 2, but considering time-effect. Partial differential equations given by

$$\frac{\partial^2 Q(x,t)}{\partial t^2} - \mathbf{C}\frac{\partial^2 Q(x,t)}{\partial x^2} + \mathbf{K}Q(x,t) = 0, \tag{7}$$

where $Q(x,t) = \begin{pmatrix} u_b(x,t) \\ u_{pzt}(x,t) \end{pmatrix}$, $\mathbf{C} = \begin{pmatrix} c_s & 0 \\ 0 & c_p \end{pmatrix}$, $\mathbf{K} = \begin{pmatrix} k_s & -k_s \\ -k_p & k_p \end{pmatrix}$, $c_p = \frac{E_p}{\rho_p}$, $c_s = \frac{E_s}{\rho_s}$, $K_p = \frac{G_a}{\rho_p}$, ρ_p is the density of the PZT sensor, ρ_s is the density of the structure, characterizes the dynamic equation.

The solutions for coupled Eq. (7) are determined by

$$u_b(x,t) = (\alpha_1 \cosh(\lambda_1 x) + \alpha_2 \sinh(\lambda_1 x) + \alpha_3 \cosh(\lambda_2 x) + \alpha_4 \sinh(\lambda_1 x)) e^{i\omega t},$$

Copyright © 2010 Asociación Argentina de Mecánica Computacional http://www.amcaonline.org.ar

$$u_p(x,t) = (\beta_1(\alpha_1 \cosh(\lambda_1 x) + \alpha_2 \sinh(\lambda_1 x)) + \beta_2(\alpha_3 \cosh(\lambda_2 x) + \alpha_4 \sinh(\lambda_1 x)))e^{i\omega t}, \quad (8)$$

where

$$\lambda_1 = \sqrt{\frac{-c_1 + \sqrt{{c_1}^2 - 4c_2}}{2}}, \qquad \lambda_2 = \sqrt{\frac{-c_1 - \sqrt{{c_1}^2 - 4c_2}}{2}},$$

$$c_1 = -\left(\frac{1}{c_s}(k_s - \omega^2) + \frac{1}{c_p}(k_p - \omega^2)\right), \; c_2 = \left(\frac{1}{c_p c_s}(k_s - \omega^2)(k_p - \omega^2) - \frac{k_p k_s}{c_p c_s}\right),$$

$$\beta_1 = \left(-\frac{c_s}{k_s}{\lambda_1}^2 + \frac{1}{k_s}(k_s - \omega^2)\right) \text{ and } \beta_1 = \left(\frac{c_s}{k_s}{\lambda_2}^2 - \frac{1}{k_s}(k_s - \omega^2)\right).$$

The constants $\alpha_1, \alpha_2, \alpha_3, \alpha_4$ can be determined by boundary conditions.

2.3 Electrical response in the PZT sensor

Electrical signatures emitted by the PZT sensor generated by mechanical deformation can be determined using the first Maxwell´s equation (Gauss law for electricity, see (Ballas, 2007)), which relates electric charge density ϱ with electric displacement D_i as

$$\varrho = \mathbf{div}(D_i). \quad (9)$$

Total electric charge accumulated in the PZT sensor is determined by

$$Q = \iiint_V \varrho dV, \quad (10)$$

where V is the volume of the PZT sensor. (Sirohi and Chopra, 2000) analyzed the PZT sensor as a capacitor due to electrical charge and discharge effects. Therefore, the voltage produced by electrodes can be obtained as

$$V_{pzt} = \frac{Q}{C_{pzt}}, \quad (11)$$

where C_{pzt} is the capacitance of the piezoelectric material (PZT) and it is calculated by

$$C_{pzt} = \frac{e_{33} l_p w_p}{h_p}, \quad (12)$$

where e_{33} is the electric permittivity and l_p is the length of the PZT sensor.

Copyright © 2010 Asociación Argentina de Mecánica Computacional http://www.amcaonline.org.ar

3 NUMERICAL EXAMPLE

In Fig. 3 it is shown a structure or rod bonded to a piezoelectric sensor by means of an adhesive layer. Table 1 shows the physical properties of the structure, PZT sensor and adhesive layer.

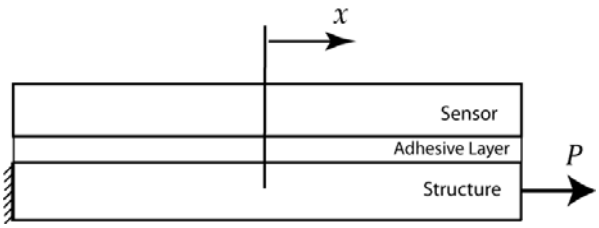

Figure 3: Structure-bonding layer-PZT sensor submitted to a P axial force.

Item	PZT Sensor	Structure	Adhesive layer
	PZT-5A	Aluminum	Araldite
Density $(kg \cdot m^{-3})$	7500	2700	7850
Young Modulus (Gpa)	120.34	70	2.84
Constant d_{15} $(C \cdot N^{-1})$	$5.84x10^{10}$	……	……
Relative permittivity	1.470	……	……
Thickness (mm)	0.2667	0.25	0.3
Length (mm)	5 *and* 15	5 *and* 15	5 *and* 15

Table 1: Physical and geometric properties

Static results shown in Fig. 6 were obtained using the definition of strain from Eq. (5). The solutions of figures **7** and 8 were obtained by means of equations **(**3) and (11). Dynamic results shown in figures 10a and 11a were obtained differentiating the analytical solutions established in Eq. (8). Figures 10b, 11b and 13 were obtained with (COMSOL, 2007). Figure 14 was determined applying equations (13) and (14).

3.1 Static results

The static problem was modeled in (COMSOL, 2007) to compare the analytical solutions obtained with the following boundary conditions: $u_b(-l/2) = 0$, $P = 20$ N, $\frac{du_p}{dx}(-l/2) = 0$, $\frac{du_p}{dx}(l/2) = 0$ (strain in the end points of the PZT sensor is zero) and $w = 15\,mm$ (width of structure, adhesive layer and PZT).

Figure 5 shows displacements obtained by finite element method using (COMSOL, 2007), and the analytical solutions shown in Eq. (5). The mesh established for the numerical model done in (COMSOL, 2007), presents 2240 triangular elements and 9282 degrees of freedom (see Fig. 4). It is possible to verify that the finite element method and analytical solutions presents a good agreement.

Copyright © 2010 Asociación Argentina de Mecánica Computacional http://www.amcaonline.org.ar

The displacements of the structure and the PZT sensor present nonlinear behavior, since distributions of strain through PZT sensor are also nonlinear (definition of strain for the sensor $\epsilon_P(x) = \frac{du_p(x)}{dx}$, for the structure $\epsilon_b(x) = \frac{du_b(x)}{dx}$, see Fig. 6). Displacement values along the length of the structure and along the PZT are different, as it is shown in the Fig. 5. When the PZT sensor was not bonded to the surface of the structure, displacements through the structure (structure in form of rod) presented linear behavior (constant strain given by $\left(\frac{d}{dx}\left(EA\frac{du}{dx}\right) = 0\right)$ as it is shown in (Kwon and Bang, 2000)). After bonding the PZT sensor in the structure, the displacements and deformations of the structure are evidently modified.

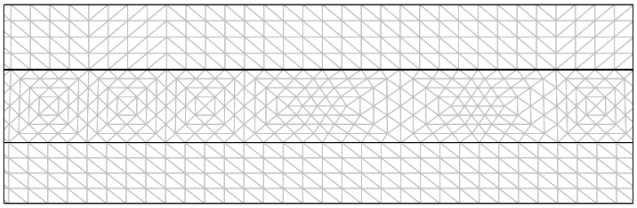

Figure 4. Mesh applied to the set with COMSOL

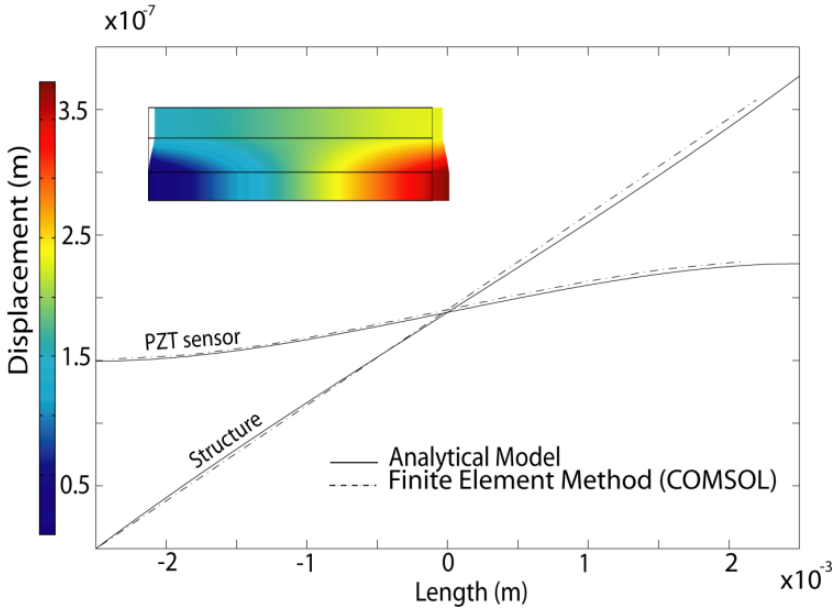

Figure 5: Displacement solutions by FEM and analytical solution for $l = 5\ mm$

3.1.1 Mechanical effects

Figure 6 shows the deformations of the structure and the PZT sensor for different thicknesses and lengths after applying the force P. In this figure the strain distribution is nonlinear for the lengths of bonding 5 mm and 15 mm, and for different thicknesses of bonding layer. Figure 6a

Copyright © 2010 Asociación Argentina de Mecánica Computacional http://www.amcaonline.org.ar

shows that the PZT sensor strain is separated of the structure strain in interval $x \in (-2.5,2.5)$. When the thickness of the adhesive layer is smaller than $h_a = 0.3\,mm$, $(h_a \in (0.1h_a, 0.9h_a))$ the strain values of the structure and PZT sensor can be considered approximately equal. Figure 6b shows that the values of strain in the adhesive interface are more effective when x $\in (-5,5)$. This represents 66.6 % of the total length adhered. It is important to denote that the length influences significantly the force transmission through the interface.

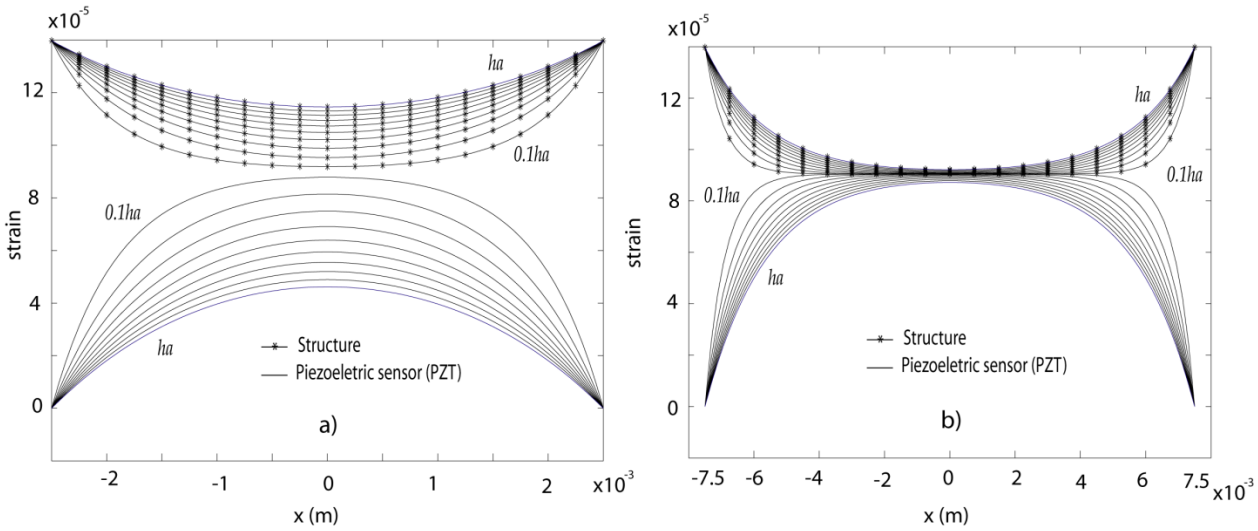

Figure 6: Analytical solutions of the deformation of the sensor and the structure, a) $l = 5\,mm$, b) $l = 15\,mm$

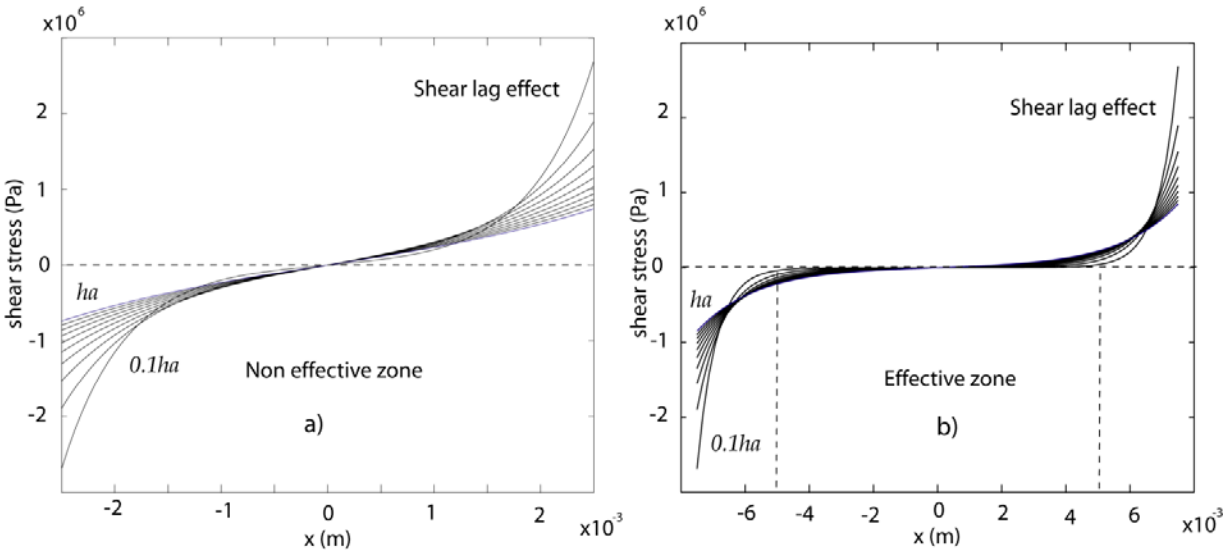

Figure 7: Analytical solutions of shear stress at the adhesive interface to a) $l = 5\,mm$, b) $15\,mm$

Figure 7 shows shear stress through the bonding interfaces for the lengths of $5\,mm$ (see Fig. 7a) and $15\,mm$ (see Fig. 7b). Shear stresses shown in Fig. 7a do not present an effective zone in which the transference of shear forces can be transmitted without distortion of the adhesive layer. In this case, the adhesive layer does not present distortion at the point $x = 0$, where the

Copyright © 2010 Asociación Argentina de Mecánica Computacional http://www.amcaonline.org.ar

mechanism of force transference is purely shearing along the interface. On the other hand, it is possible to verify in Fig. 7b an effective zone where shear forces deform the adhesive layer uniformly. This means that there is no distortion of the adhesive layer (shear forces are null). In the effective zone, the effect of displacement shown in Fig. 1 (displacement of the structure bigger than displacement in PZT at a point x), will not be presented through the entire interface, since the displacements and deformations in the effective zone are equal. In this Fig. it can be observed that the shear lag effect is presented only in the ends of the interface (see (Balla and Soh, 2004)).

Axial deformation produces a symmetrical strain distribution (see Fig. 6) through the bonding interface. This principle can be used to determine debonding (Xu and Liu, 2002) and simulate debonding with the decrease of the stiffness of the adhesive layer dividing the electrode of the PZT sensor (in this study this will not be considered).

3.1.2 Electrical effects

Figure 8 was obtained by means of Eq. (11), the electric displacement was calculated with the strain of the sensor (see Eq.(2)). This figure compares electric potential (electrical signature emitted) generated by the PZT sensor of two lengths and for different cases of adhesive thickness. Results indicate that when the thickness of the adhesive layer is bigger, the electric potential emitted by the sensor is smaller, as it was presented by (Han et al. 2008). Furthermore, if the piezoelectric sensor is longer, the electric potential is bigger. In all cases of adhesive thickness the electric potential emitted by the PZT sensor of length 15 mm is bigger than the electric potential emitted by the sensor of 5 mm.

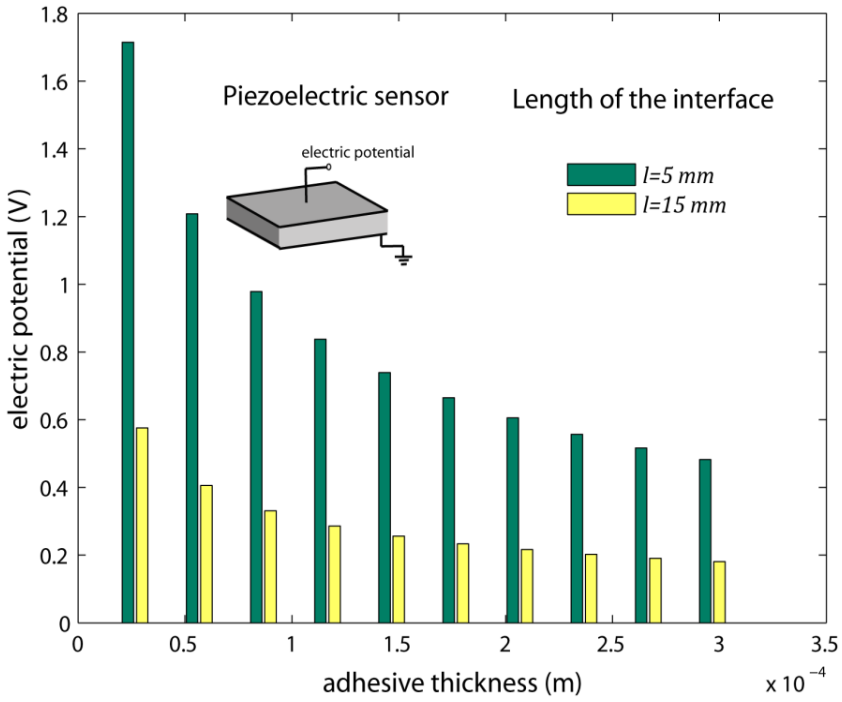

Figure 8. Adhesive thickness effects on electric potential

Copyright © 2010 Asociación Argentina de Mecánica Computacional http://www.amcaonline.org.ar

If a fully adhered sensor is partially debonded in the ends, the electric potential generated by sensor under the same conditions of force will begin to decrease, because electrical signatures are smaller when the length of the PZT sensor is smaller. If the PZT sensor is partially debonded, it can emit electrical signatures due to local deformation in the structure (the PZT sensor is also deformed).

3.2 Dynamic results

Dynamic problem of Fig. 3 was proposed and solved for two cases: PZT sensor fully bonded (solved with the analytical solution, see Eq. (8)) and PZT sensor partially bonded (solved with the numerical solution obtained by FEM). The analytical solution was determined with the following boundary conditions, such that $u_b(0) = 0$, $P = 20\sin(\omega t)$, where $\omega = 20\ Hz$ is the excitation frequency, $\frac{du_p}{dx}\left(-\frac{l}{2}\right) = 0$, $\frac{du_p}{dx}\left(-\frac{l}{2}\right) = 0$ and $w = 15\ mm$. In such a case the length of the set shown in Fig. 3 is $30\ mm$. The physical and geometrical properties of the problem are shown in Table 1.

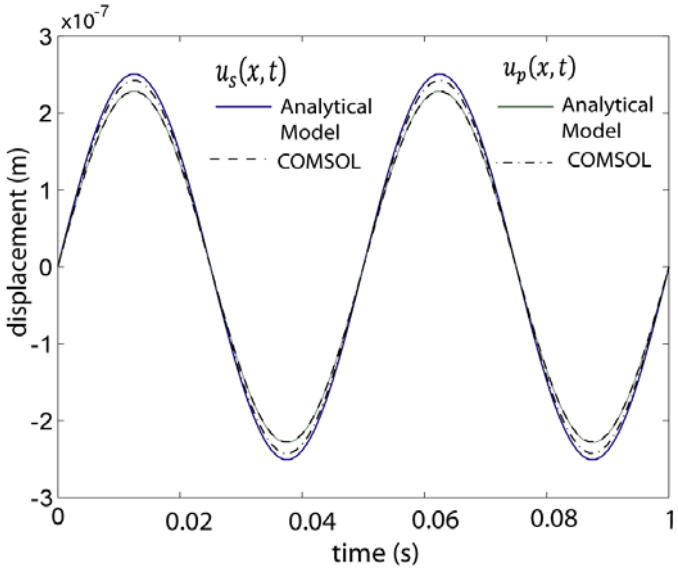

Figure 9: Displacements at $x = l/2$ to $t \in (0,1)$

The numerical solution of the problem shown in Fig. 3 was obtained using (COMSOL, 2007) with a finite elements mesh (see Fig. 4) of 2240 triangular elements and 9282 degrees of freedom. This model was established to compare with the dynamic analytical solution shown in Eq. (8). Figure 9 shows the displacements of the structure and the sensor at the point $x = l/2$. The analytical displacement solutions present a satisfactory approximation with respect to numerical solutions. In Fig. 9 displacement can be observed that the displacement of the point $x = l/2$ of the structure is bigger than the displacement of the PZT in the same point. This means that one part of the deformation energy remains in the adhesive layer when forces are transmitted through the interface.

Copyright © 2010 Asociación Argentina de Mecánica Computacional http://www.amcaonline.org.ar

3.2.1 Dynamic results with debonding (5 mm)

Figures 10 and 11 show the deformations of the structure and of the PZT sensor for two cases, fully bonded and partially bonded (25 mm $bonded$). In Fig. 10 one can observe that when the PZT sensor is debonded, the strains of the structure increase in the debonded area. This shows that the measures of strain obtained by the PZT sensor are smaller than real deformations produced in the structure and smaller than the deformations outside of the bonded section (structure-adhesive layer-PZT).

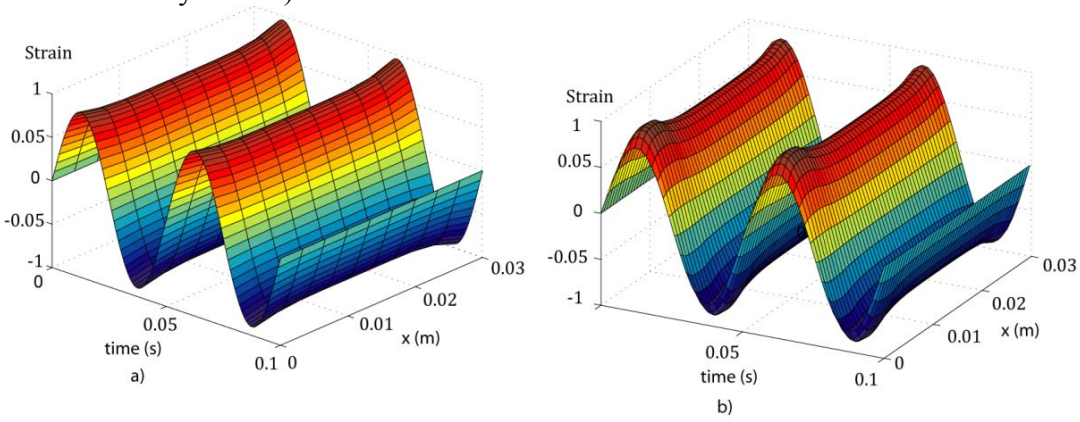

Figure 10: Strain of the structure, a) sensor fully bonded ($\boldsymbol{l = 30\ mm}$), b) sensor partially bonded ($\boldsymbol{l = 25\ mm}$)

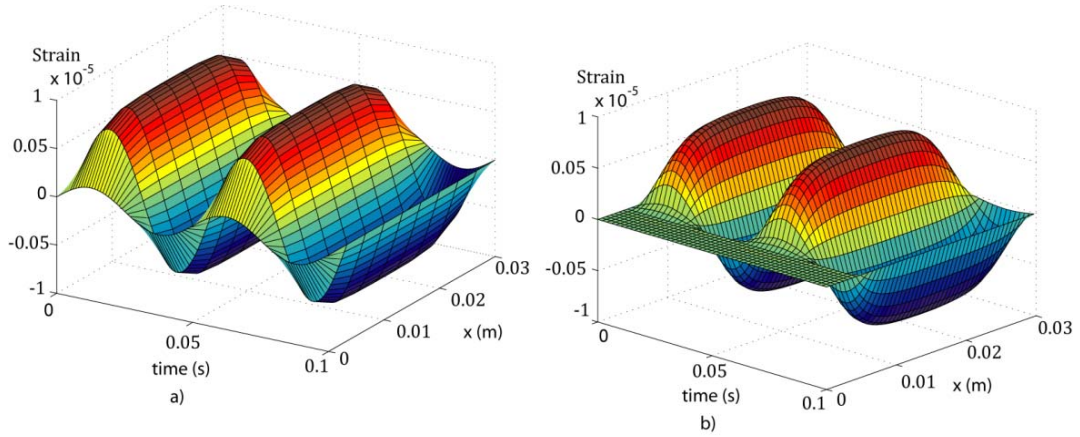

Figure 11: Strain of the sensor, a) sensor fully bonded ($l = 30\ mm$), b) sensor partially bonded ($l = 25\ mm$)

Strains through the sensor, caused by applying force in determined period of time, t ∈ (0,0.1) s, are shown in Fig. 11. Figures 11a and 11b correspond to the deformations of the PZT sensor, when the PZT sensor is fully bonded and partially bonded to the structure (debonded 5 mm in left end). In Fig. 11b one can observe that the deformation in the area, in which is localized the debonding, presents null strain.

Due to the debonding in the end, the sensor loses performance (energy relation input-output) and effectiveness (force transference along the sensor) when it performs the task of monitoring.

Copyright © 2010 Asociación Argentina de Mecánica Computacional http://www.amcaonline.org.ar

The mechanical effects of the debonding will be reflected in the changes of deformation near to the debonded end of the PZT sensor. Failure or rupture by fatigue could be generated in time by this deformation due to the action of periodical forces which act in the debonded section. The debonded section of PZT sensor will act as a short beam submitted to periodical bending forces (see Fig. 12 left end)

3.2.2 Electrical results with debonding ($5, 10, 15, 20, 25\ mm$)

Figure 12 shows the set structure-adhesive layer-sensor. In this case one end is not fully adhered in this figure, d represents the disjoined of the structure and the sensor, l_e is the effective length of adherence in the sensor and the structure.

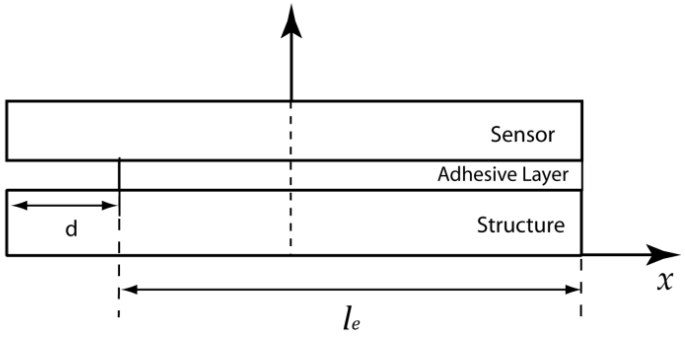

Figure 12: Set with one partially debonded end

Electric charge generated by the sensor to the different cases of adhesion is shown in Fig. 13. Electric charge values were obtained with (COMSOL, 2007).

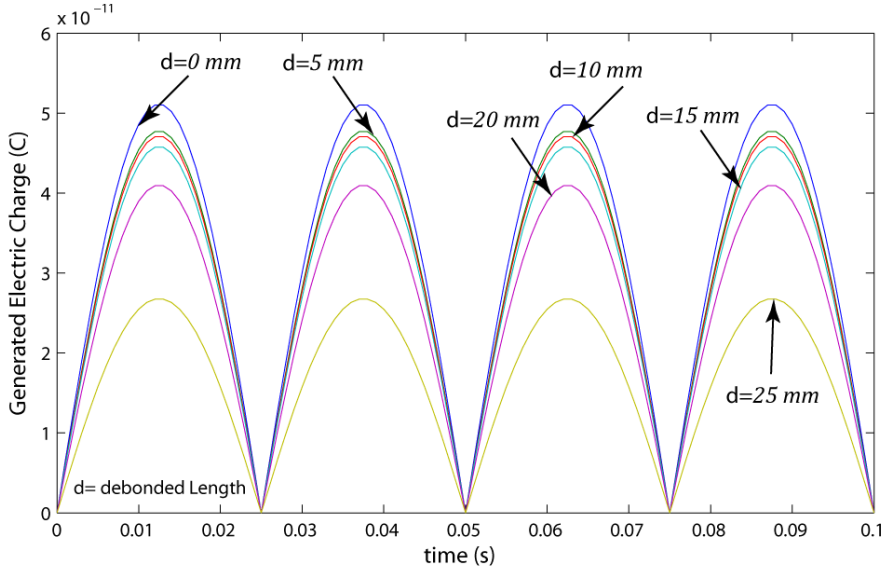

Figure 13: Electrical charge generated by the PZT sensor in different cases of debonding.

Copyright © 2010 Asociación Argentina de Mecánica Computacional http://www.amcaonline.org.ar

In Fig. 13 it can be observed that when the lengths of adhesion are smaller, the generated electric charge by the sensor is smaller. It is important to mention that the debonded sensor emits electrical signatures caused by the local deformation of the structure. This means that the PZT sensor presents functionality when it is partially bonded. However, when a sensor presents debonding, the disjoint of the sensor is considered as a failure. The failure could be evaluated by the performance of the sensor taking into account the decrease of the electrical signatures emitted.

In this study, it is established a relation of performance which permits to measure the electric charge percentage respect to the initial measurement of electric charge generated by the PZT sensor, in same dynamic conditions. Therefore, we establish the electrical charge performance (P_C) in two measures of electrical charge as

$$P_C = \frac{Vmax_{iC}}{Vmax_C}, \tag{13}$$

where $Vmax_C$ is the maximum value of electrical charge obtained initially to a periodical excitation, $Vmax_{iC}$ is the maximum value of electrical charge obtained after a time in the same excitation conditions. Also it is established a relation of adhesion effective percentage (P_e) with the effective length of the following form

$$P_e = \frac{L_{eI}}{l}, \tag{14}$$

where l is the initial length of adhesion and L_{eI} is the effective length of adhesion after dedonding the sensor. Relations established in equations (13) and (14) are shown in Fig. 14. In this figure it can be observed that the electrical charge performance (P_C) decreases slower than adhesion effective percentage (P_e).

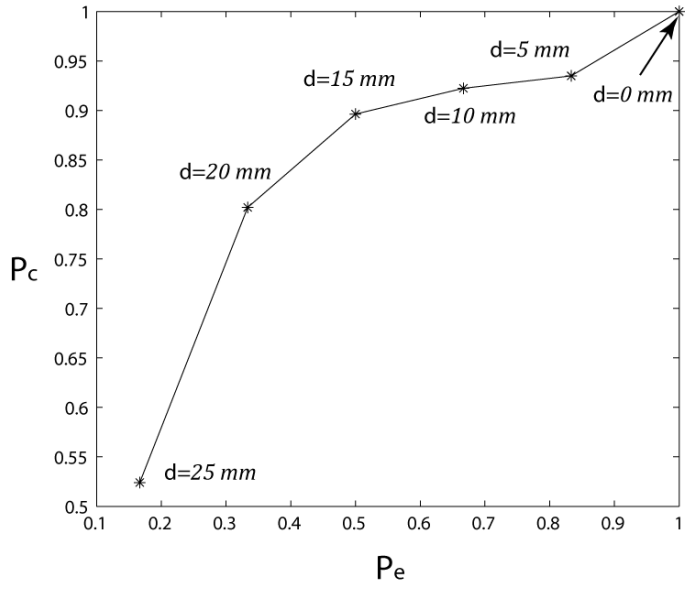

Figure 14: Adhesion effective percentage ($\boldsymbol{P_e}$) vs electrical charge performance ($\boldsymbol{P_c}$)

Copyright © 2010 Asociación Argentina de Mecánica Computacional http://www.amcaonline.org.ar

4 CONCLUSIONS

In this study it was verified that the properties of adhesive layer present effects on the mechanical and electrical behavior of the structure and the PZT sensor. Deformations along bonded interface in the sensor and the structure present a nonlinear distribution of the strain, and displacements determined in both parts (structure and PZT sensor) also presented nonlinear behavior. Electric potential emitted by PZT sensor when the structure is submitted to a known force is modified when the thickness of the adhesive layer varies. The mechanical effects of the adhesive thickness were reflected on strains and electrical effects were reflected on electric potential generated by the PZT sensor. Shear stresses were affected by the length of the sensor. For instance, when the length of the PZT sensor is larger, the force transference is realized by means of deformation of effective zone, in which deformations are equal. Transmitted shear forces create an effect on the end of the PZT sensor, where shear stresses are bigger in the ends of the adhered surface. On the other hand, if PZT sensors have smaller lengths the mechanism to transmit forces is completely via shear stress through the interface.

When the PZT sensor is debonded, structure strains increase out of the adhered interface and PZT sensor strains are null in the disjoint section. For different cases of debonding, electric charge generated by the sensor diminishes as the value of debonding of the adhesive interface becomes bigger. Relations established (P_C and P_e) for the cases of debonding show that the PZT sensor does not lose effectiveness when it is debonded. For example, when the PZT sensor is 30 % debonded the effectiveness of the electric charge is 90% and when the PZT sensor is 65 % debonded the effectiveness of the electric charge is 80%. If the PZT sensor is partially debonded, it can emit electrical signatures, due to the local deformation in the structure, the PZT sensor is also deformed. This demonstrates that it is necessary to evaluate the performance of the sensor for determining optimal operation conditions and not to consider the debonding as failure to such a point that it presents minimum effectiveness. The knowledge of the effects of the adhesive layer can help to keep the PZT sensor health monitoring as also the structural health monitoring.

FEM (using (COMSOL, 2007)) was necessary for determining the solution in the cases of debonding. Since that the analytical models obtained were proposed for the interfaces (structure/adhesive and adhesive/sensor) fully adhered. Numerical results will present a satisfactory approximation with respect to analytical solutions determined.

ACKNOWLEDGMENT

The authors are grateful to CAPES (Coordenação de Aperfeiçoamento de Pessoal de Nível Superior) for the financial support. The authors also extend a sincere thanks to Santander bank (Brazil) scholarship for the financial support given.

Copyright © 2010 Asociación Argentina de Mecánica Computacional http://www.amcaonline.org.ar

REFERENCES

Allik H. and Hughes T. J. R. Finite element method for piezoelectric vibration. *International Journal for Numerical Methods in Engineering*, 2:151-157. 1970.

Ballas, R. G. *Piezoelectric multilayer beam bending actuators: static and dynamic behavior and aspects of sensor integration*. Springer-Verlag, 2007.

Bendary I., Elshafei M. A., and Riad A. M. Finite element model of smart beams with distributed piezoelectric actuators. *Journal of Intelligent Material Systems and Structures,* 21(7): 747-758, 2010.

Benjeddou A. and Trindale M. A. Piezoelectric active vibration control of damped sandwich beams. *Journal of Vibration and Acoustics*, 246:653–677. 2001.

Bhalla S. and Soh C. K. Structural health monitoring by piezo-impedance transducers: I modeling. *Journal of Aerospace Engineering ASCE*, 17(4):154-165, 2004a.

Bhalla S. and Soh C. K. Structural health monitoring by piezo-impedance transducers: II applications. *Journal of Aerospace Engineering ASCE*, 17(4):166-175, 2004b.

Chen C., Wang, X., and Shen Y. Finite element approach of vibration control using self-sensing piezoelectric actuators. *Computers & Structures*, 60(3):505-512, 1996.

COMSOL. Reference manual for COMSOL 3.5, COMSOL LAB, Stockholm, 2007. www.comsol.se.

Crawley E. and Luis J. Use of piezoelectric actuators as elements of intelligent structures. *AIAA Journal,* 25(10):373-1385, 1986.

Diamanti K., Soutis C., and Hodgkinson J. M. Piezoelectric transducer arrangement for the inspection of large composite structures. *Composites Part A: Applied Science and Manufacturing*, 38(4):1121-1130, 2007.

Giurgiutiu V. and Zagrai A. N. Characterization of piezoelectric wafer active sensors. *Journal of Intelligent Material Systems and Structures*, 11(12):959-976, 2000.

Han L., Wang X. D., and Sun Y. The effect of bonding layer properties on the dynamic behaviour of surface-bonded piezoelectric sensors. *International Journal of Solids and Structures*, 45(21):5599-5612. 2008.

Kwon Y. W. and Bang H. *The Finite Element Method Using MATLAB*, Second Edition. CRC Press, 2000.

Liang L., Sun F. P., and Rogers C. A. Coupled electro-mechanical analysis of piezoelectric ceramic actuator-driven systems – Determination of the Actuator Power Consumption and

Copyright © 2010 Asociación Argentina de Mecánica Computacional http://www.amcaonline.org.ar

System Energy Transfer. In: *Proceedings of Smart Structures and Materials '93*, SPIE, Albuquerque, NM. 286–298. 1993.

Liang L., Sun F. P., and Rogers C. A. Electro-mechanical impedance modeling of active material systems. *Smart Materials and Structures*, 5(2):171–186. 1996.

Park G., Cudney H., and Inman D. J. Impedance-based health monitoring of civil structural components. *ASCE Journal of Infrastructure Systems*, 6(4):153–160, 2000.

Pi ceramics. Catalogue of piezoelectric actuators and sensors. http://www.piceramic.com

Pietrzakowski M. Multiple piezoceramic segments in structural vibration control. *Journal of Theoretical and Applied Mechanics,* 38:35–50. 2000.

Ritdumrongkul S., Abe M., Fujino Y., and Miyashita T. Quantitative health monitoring of bolted joints using a piezoceramic actuator sensor. S*mart Materials and Structures*, 13(1):20-29, 2004.

Sirohi J. and Chopra I. Fundamental Understanding of Piezoelectric Strain Sensors. *Journal of Intelligent Material Systems and Structures*, 11(4):246-257, 2000.

Sun F. P., Chaudhry Z., Rogers C. A., Majmundar M., and Liang C. Automated real-time structure health monitoring via signature pattern recognition. In: *Proceedings of SPIE Conference on Smart Structures and Materials*, San Diego, California, 2443:236-247, 1995.

Tanasoiu V., Miclea C., and Tanasoiu C. Nondestructive testing and piezoelectric ultrasonics transducer for wood and built in wooden structures. *Journal of Optoelectronics and Advanced Materials*, 4(4):949-957, 2002.

Tylinkowski A. Stabilization of beam parametric vibrations. *Journal of Theoretical and Applied Mechanics,* 31:657–670, 1993.

Tzou H. S. and Tseng C. I. Distributed Piezoelectric Sensor/Actuator Design for Dynamic Measurement/Control of Distributed Parameter Systems: A Piezoelectric Finite Element Approach. *Journal of Sound and Vibration*, 138(1):1734, 1990.

Tzou H. S. and Ye R. Analysis of piezoelastic structures with laminated piezoelectric triangle shell elements. *AIAA Journal*, 34(1):110–115. 1996.

Xu J. F., Yang, Y. W., and Soh C. K. Electromechanical impedance-based structural health monitoring with evolutionary programming. *Journal of Aerospace Engineering*, 17(4):182-93, 2004.

Copyright © 2010 Asociación Argentina de Mecánica Computacional http://www.amcaonline.org.ar

Xu Y. G. and Liu G. R. A modified electro-mechanical impedance model of piezoelectric actuator-sensors for debonding detection of composite patches. *Journal of Intelligent Material Systems and Structures*, 13(6):389–396, 2002.

Yang S. and Ngoi B. General sensor equation and actuator equation for the theory of aminated piezoelectric plates. *Smart Materials and Structures.* 8:411-415, 1999.

Yang Y. W., Bhalla S., Wang C., Soh C. K., and Zhao J. Monitoring of rocks using smart sensors. *Tunnelling Underground Space Technology*, 22(2):206-21, 2006.

Copyright © 2010 Asociación Argentina de Mecánica Computacional http://www.amcaonline.org.ar